

Electronic Supplementary Material (ESI)

Dual-Nitrogen-Source Engineered Fe-N_x Moieties as A Booster to Oxygen Electroreduction

Dan Wang,^a Lihui Xiao,^a Peixia Yang,^{*a} Zhengrui Xu,^b Xiangyu Lu,^c Lei Du,^{*a} Oleg Levin,^d Liping Ge,^a Xiaona Pan,^{a, b} Jinqiu Zhang^a and Maozhong An^a

a MIIT Key Laboratory of Critical Materials Technology for New Energy Conversion and Storage, School of Chemistry and Chemical Engineering, Harbin Institute of Technology, Harbin, 150001 China.

b Department of Chemistry, Virginia Tech, Blacksburg, VA 24061, USA

c ZhuHai Coslight Battery Co., Ltd., ZhuHai, 519180, China.

d St. Petersburg State University, 7/9 Universitetskaya Nab., St. Petersburg, 199034, Russian Federation.

*E-mail: yangpeixia@hit.edu.cn, lei.du@hit.edu.cn

Optimization of the ratios of precursors

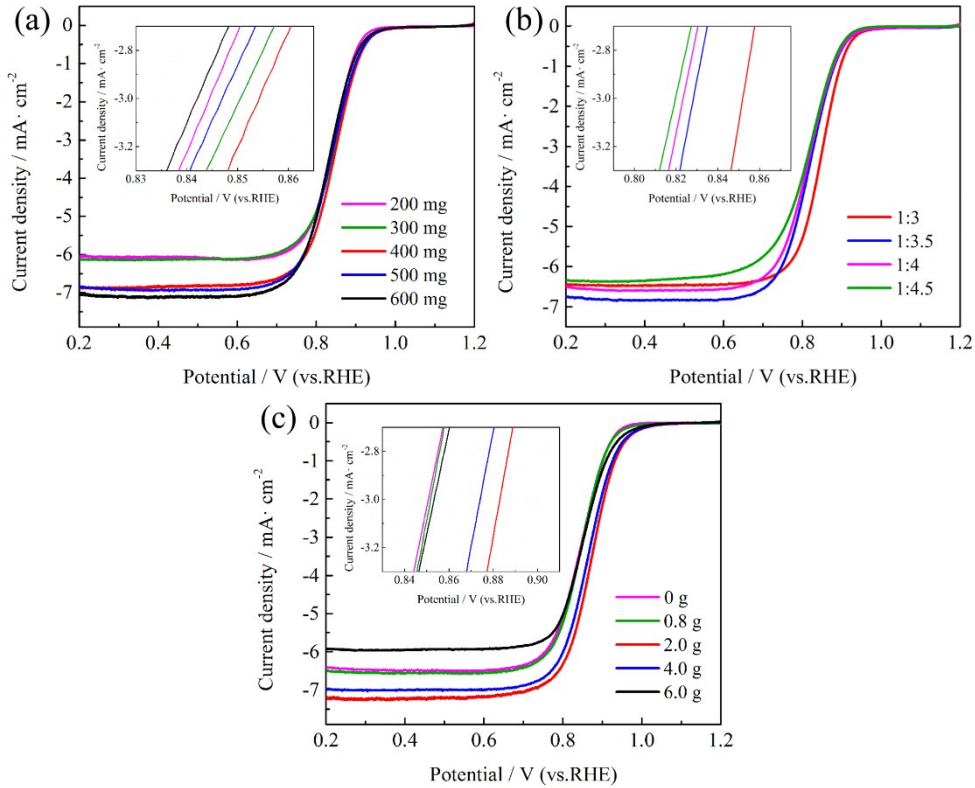


Fig. S1 (a) the mass of KB, (b) the molar ratio of Fe:Phen and (c) the mass of urea on the ORR activity of the Fe-based catalyst, respectively. (inset: partially enlarged figure)

In order to investigate the influence of the mass of KB support on the ORR activity, a series of samples were prepared with different mass of KB in precursors (200 mg, 300 mg, 400 mg, 500 mg, 600 mg). Initially, the ORR performance in terms of the half-wave potential is improved as mass of KB increasing. However, once the mass of KB is more than 400 mg, the ORR activity inversely decreases, indicating the optimum mass of KB is 400 mg in our cases.

In general, each iron ion can coordinate with three Phen molecules. As for the optimal ratio of Fe:Phen, In order to ensure that all Fe ions can coordinate with the phen molecules, we prepared the catalysts with a controlled molar ratio of 1:3, 1:3.5, 1:4, 1:4.5, respectively. Intriguingly, the Fe-based catalyst presents an optimal performance when the Fe:phen molar ratio is controlled by 1:3.

As for the optimal mass of urea, we prepared samples by adding different amount of urea in precursors to optimize the mass of urea (0 g, 0.8 g, 2.0 g, 4.0 g, 6.0 g). Initially, the ORR performance is enhanced as the mass of urea increasing. However, once the mass of urea is more than 2.0 g, the ORR activity inversely decreases, demonstrating that the optimum mass of urea is 2.0 g in the process of synthesis.

Optimization of pyrolysis temperature

In order to investigate the influence of the pyrolysis temperature on the ORR activity of catalysts, the precursors were pyrolyzed at different temperatures (700-900 °C). The SEM images of Fe-N-C-700 and Fe-N-C-900 display the similar granular-like carbon morphology with Fe-N-C-800 (Fig. S2).

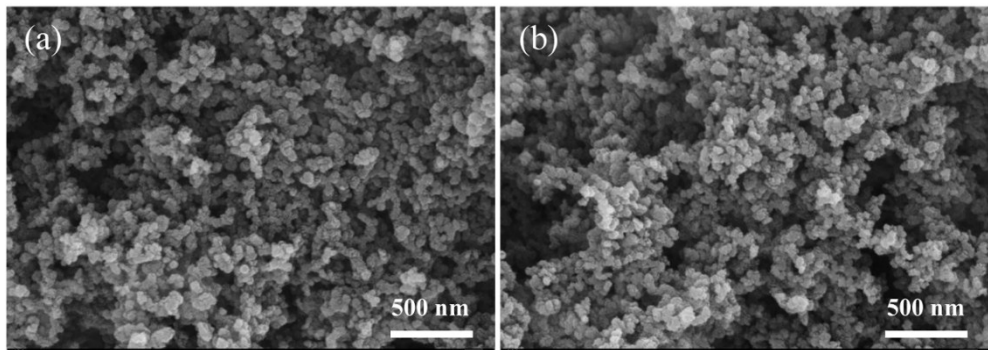


Fig. S2 SEM images of (a) Fe-N-C-700 and (b) Fe-N-C-900.

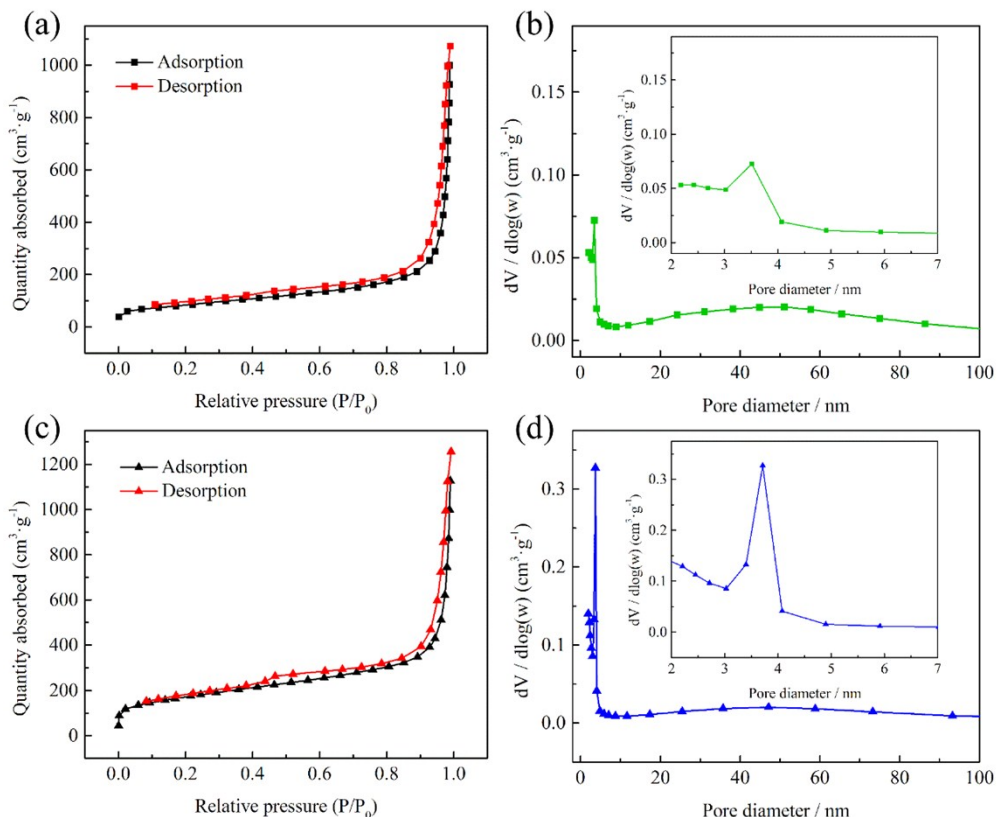


Fig. S3 Nitrogen adsorption-desorption isotherm and pore size distribution of (a, b) Fe-N-C-700 and (c, d) Fe-N-C-900. The enlarged pore size distribution was shown as inset.

The specific surface areas of Fe-N-C-700 and Fe-N-C-900 were $302.2 \text{ m}^2 \text{ g}^{-1}$ and $616.6 \text{ m}^2 \text{ g}^{-1}$, which indicates that higher pyrolysis temperature tends to enlarge the specific surface area (Fig. S3). The pore size distribution is both mainly concentrated around 4 nm like Fe-N-C-800 (inset of Fig. S3 b and d), which is beneficial to the mass

transfer in the ORR process.

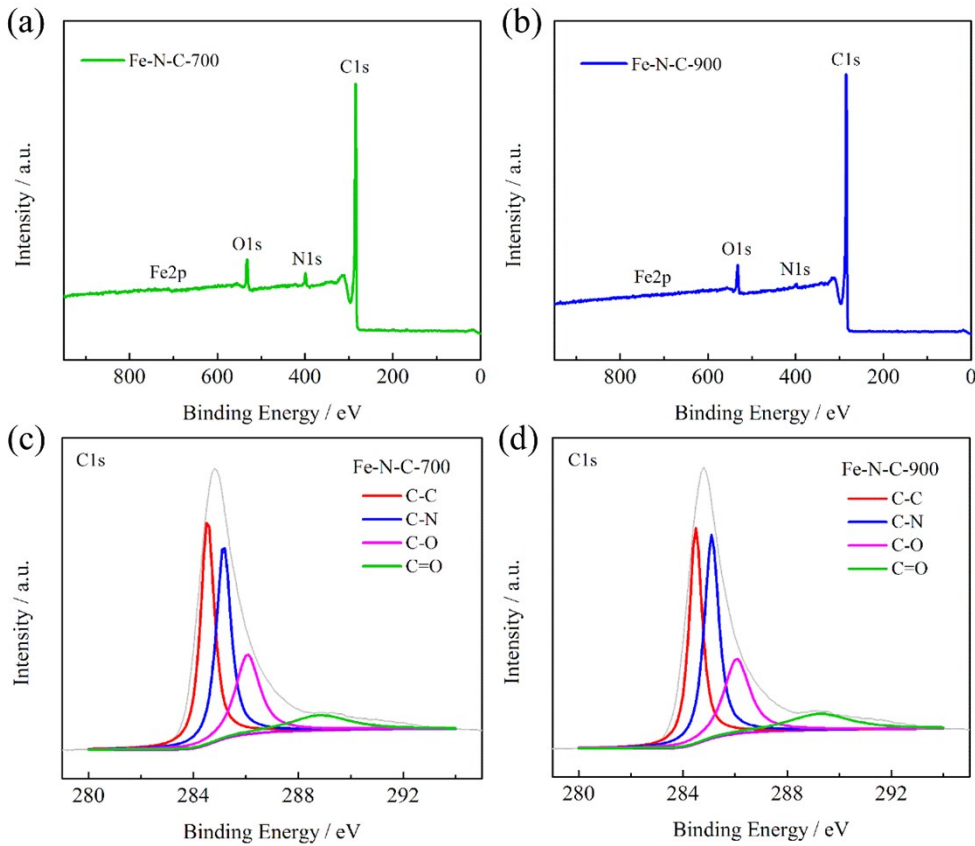


Fig. S4 XPS survey spectrum and high-resolution C 1s XPS spectra of (a) Fe-N-C-700 and (b) Fe-N-C-900.

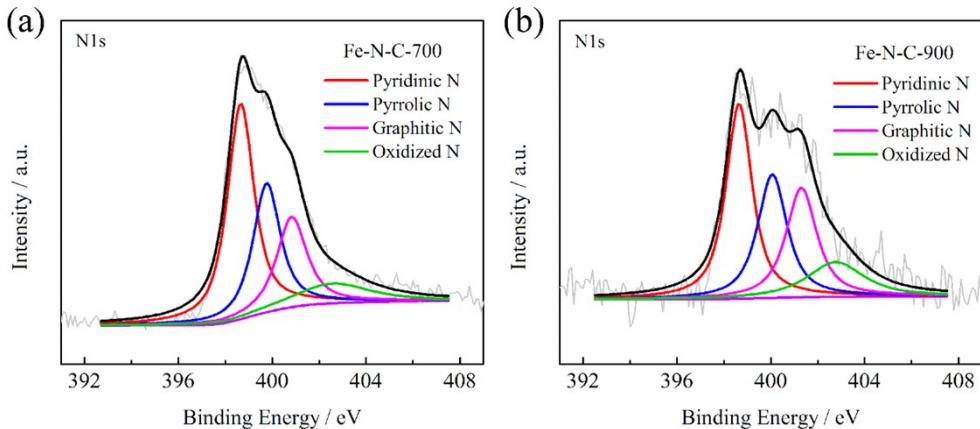


Fig. S5 High-resolution N 1s XPS spectra of (a) Fe-N-C-700 and (b) Fe-N-C-900.

To determine the elements and compositions of the catalysts, the results of XPS were presented in the Fig. S4 and S5. The coexistence of C, N, O, Fe were confirmed in the survey spectrum (Fig. S4a and b). The signal of Fe in the Fe-N-C-900 was too weak to be detected, implying its lower iron concentration on the nearface. The C1s spectrum could be deconvoluted to C-C, C-N, C-O and C=O, respectively (Fig. S4c and d). The content of nitrogen decreased from 3.22 at% of Fe-N-C-700, 2.39 at% of Fe-N-C-800

and 1.22 at% of Fe-N-C-900, demonstrating that the nitrogen would exaporate at high annealing temperature. The high-resolution N 1s spectra are deconvoluted to pyridinic N, pyrrolic N, graphitic N and oxidized N, respectively.(Fig. S5a and b) The overall fractions of pyridinic N/Fe-N in Fe-N-C-700 (42.71%) and Fe-N-C-900 (36.26%) were both lower than that of Fe-N-C-800, which would lead to the inferior ORR performance.

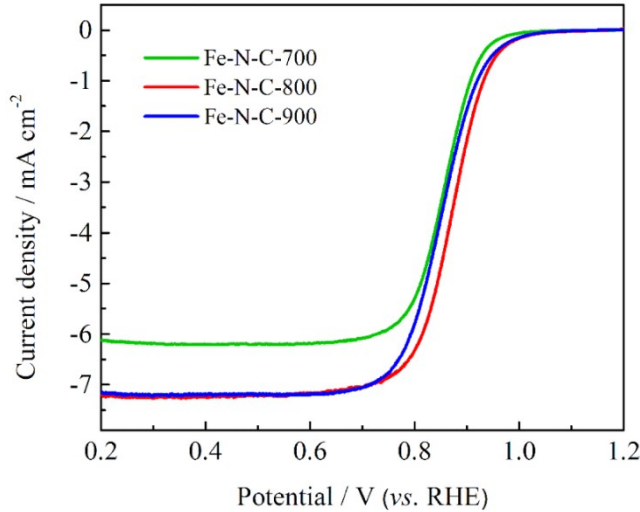


Fig. S6 ORR polarization curves of Fe-N-C-700, Fe-N-C-800 and Fe-N-C-900.

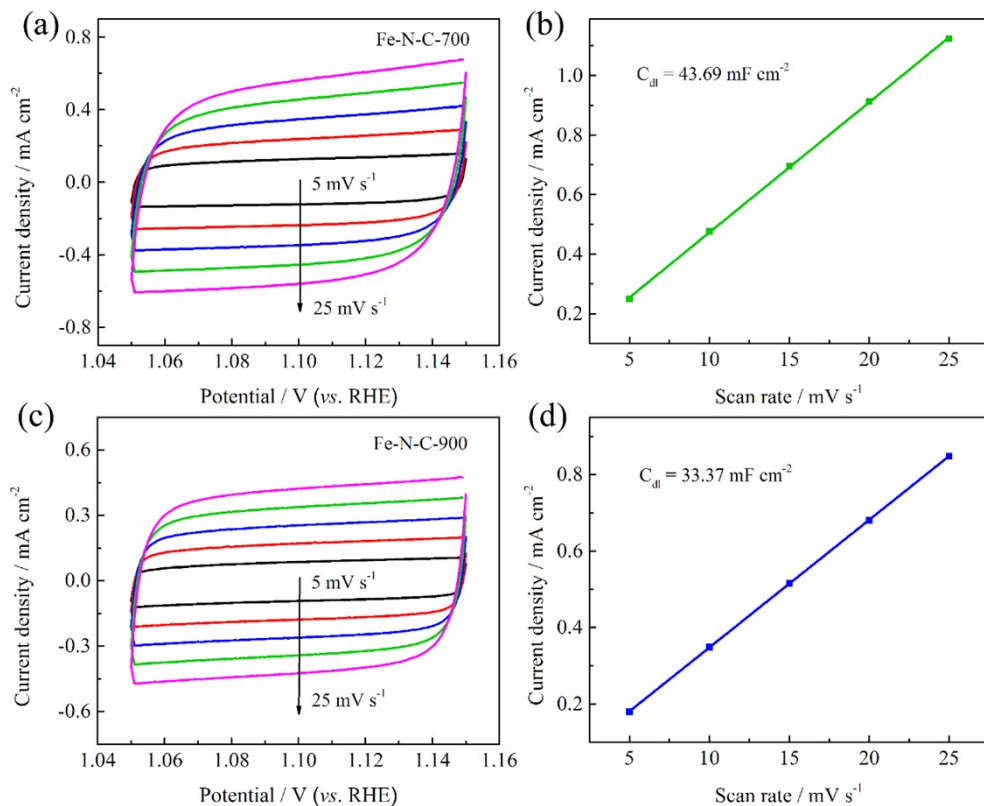


Fig. S7 CV curves at scan rates of 5,10,15,20 and 25 mV s⁻¹ in O₂-saturated 0.1 M KOH and the corresponding current density taken at 1.10 V for (a, b) Fe-N-C-700, (c,d) Fe-

N-C-900.

To further verify the above results, the ORR activity of the Fe-N-C-700 and Fe-N-C-900 are further investigated (Fig. S6). The E_{onset} and $E_{1/2}$ of Fe-N-C-700 and Fe-N-C-900 are slightly inferior compared with those of Fe-N-C-800. In addition, the C_{dl} is 43.69 mF cm⁻² of Fe-N-C-700 and 33.37 mF cm⁻² of Fe-N-C-900, slightly lower than that of Fe-N-C-800, suggesting a larger ECSA in Fe-N-C-800. (Fig. S7). To sum up, the optimum pyrolysis temperature for catalyst preparation is 800 °C.

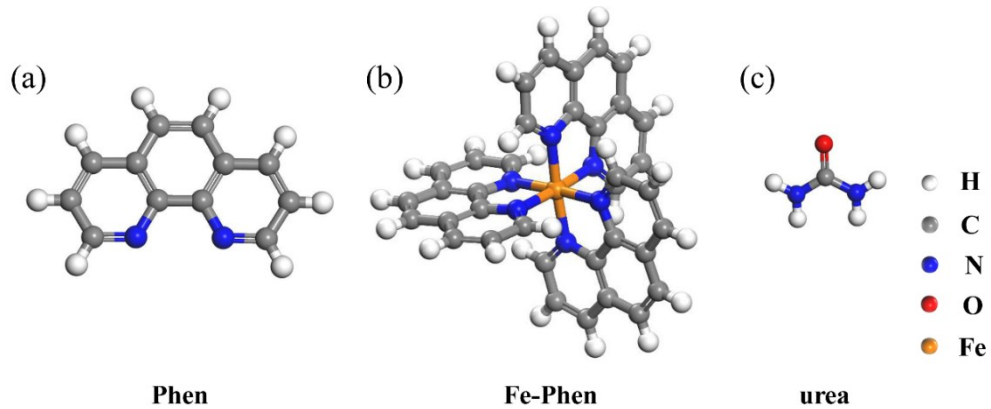


Fig. S8 Molecular structures of (a) Phen, (b) Fe-Phen and (c) urea.

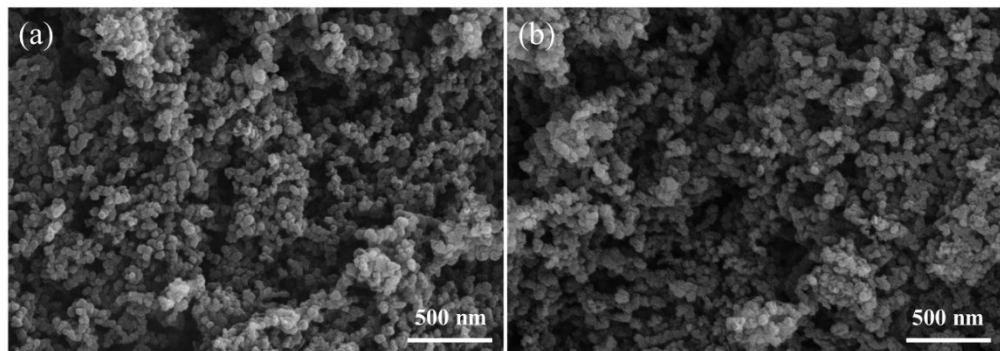


Fig. S9 SEM images of (a) precursor KB and (b) Fe-N-C-800.

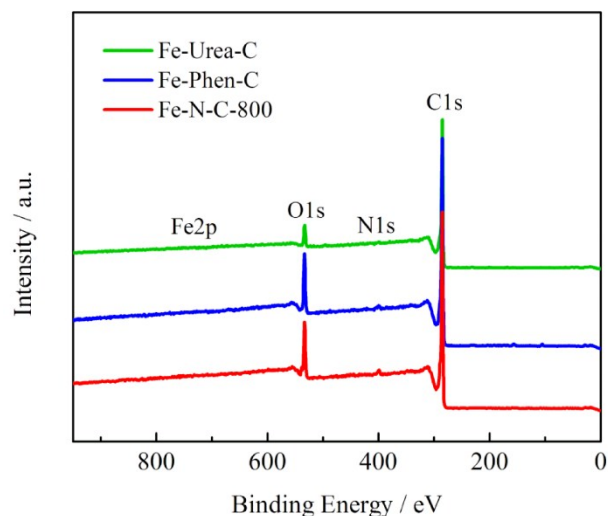


Fig. S10 XPS survey spectrum of Fe-Urea-C, Fe-Phen-C and Fe-N-C-800.

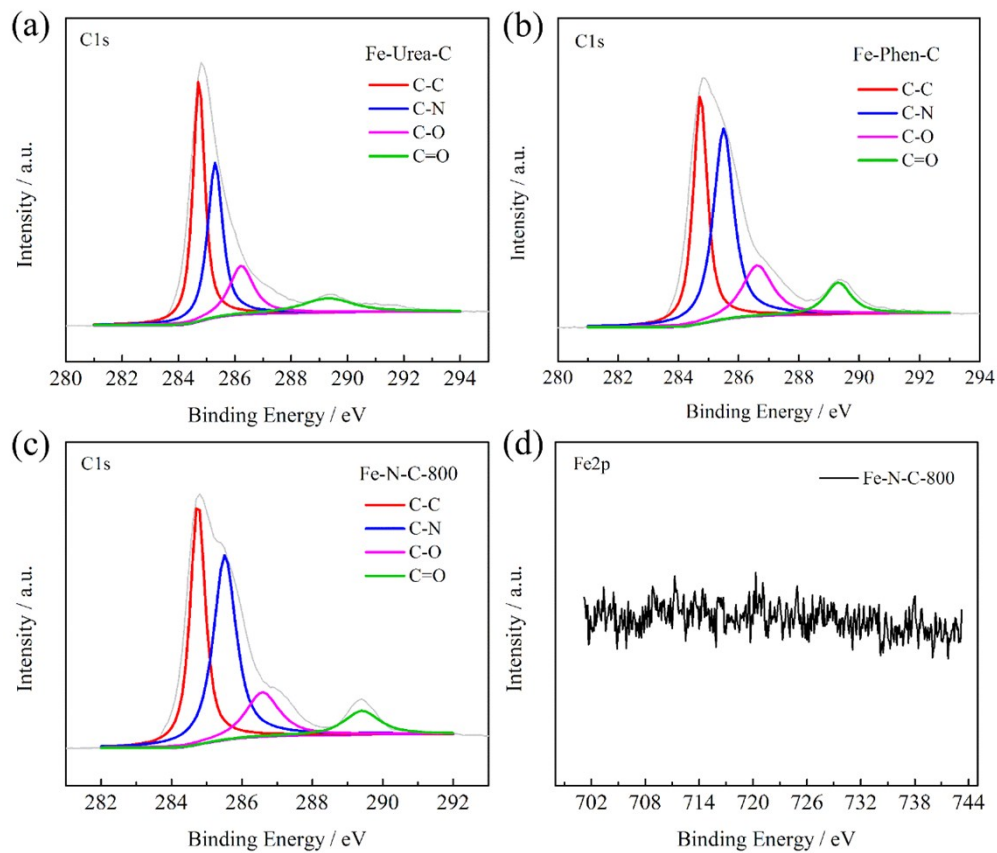


Fig. S11 High-resolution C 1s XPS spectra of (a) Fe-Urea-C, (b) Fe-Phen-C, (c) Fe-N-C-800 and (d) high-resolution Fe 2p XPS spectra of Fe-N-C-800.

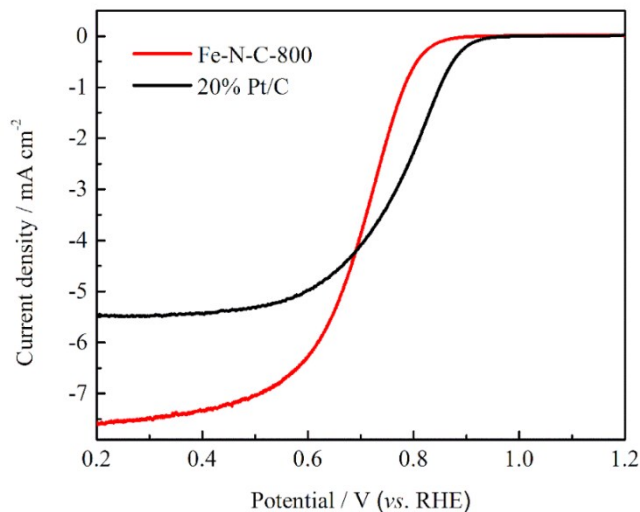


Fig. S12 ORR polarization curves of Fe-N-C-800 and 20% Pt/C in 0.1 M HClO₄.

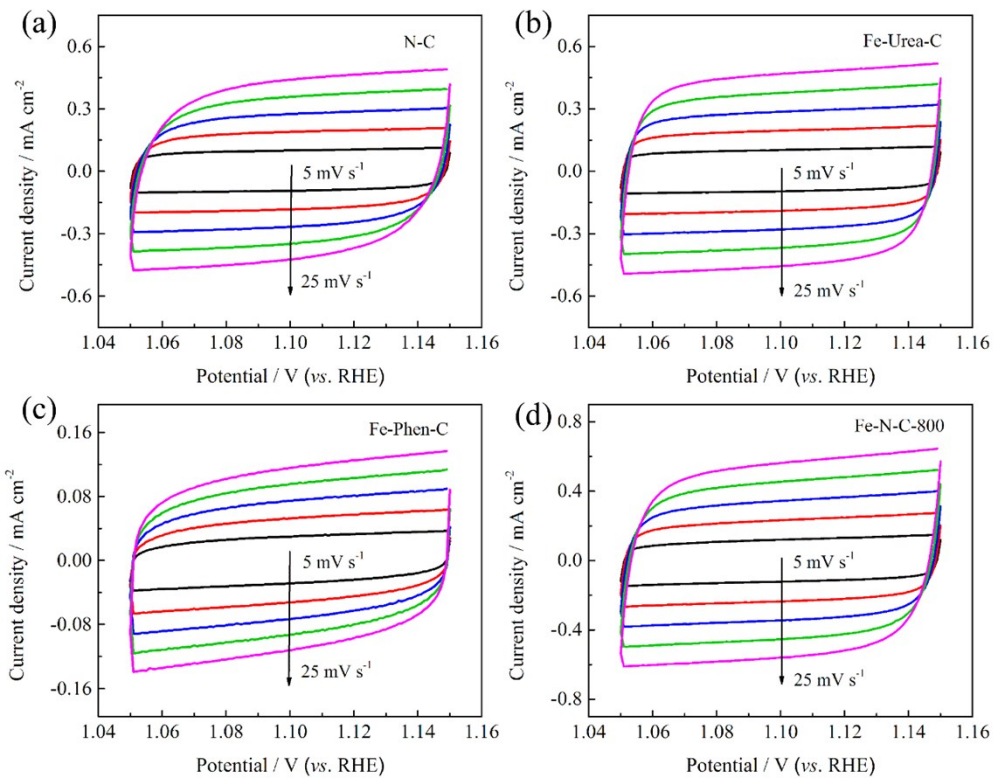


Fig. S13 CV curves of (a) N-C, (b) Fe-Urea-C, (c) Fe-Phen-C, and (d) Fe-N-C-800 at scan rates of 5, 10, 15, 20 and 25 mV s⁻¹ in O₂-saturated 0.1 M KOH.

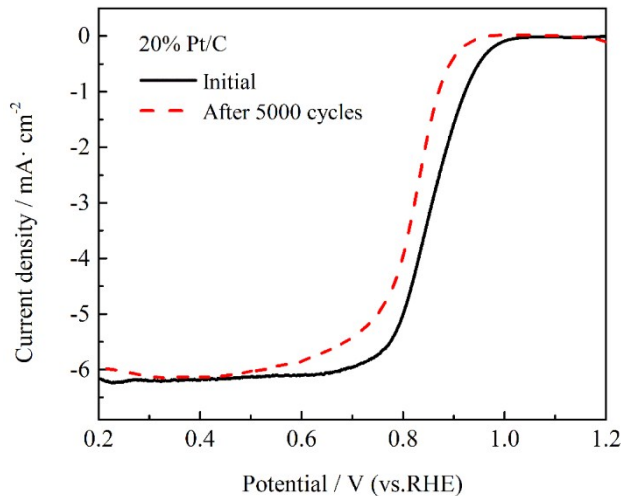


Fig. S14 ORR polarization curves before and after 5000 cycles of 20% Pt/C at 1600 rpm with a scan rate of 10 mV s⁻¹.

Table S1. The content of C, N, O and Fe of the prepared catalysts obtained from XPS.

	Atomic Concentration %				Mass Concentration %			
	C	N	O	Fe	C	N	O	Fe
Fe-Urea-C	93.38	0.97	5.64	0.01	91.47	1.11	7.36	0.06
Fe-Phen-C	86.79	1.52	11.69	0	83.35	1.70	14.95	0
Fe-N-C-800	86.80	2.39	10.58	0.24	82.84	2.66	13.46	1.05

Table S2. The content of Different types of N (%) for the prepared catalysts obtained from XPS.

sample	pyridinic N	pyrrolic N	graphitic N	oxidized N
Fe-Urea-C	32.75	25.59	21.08	20.58
Fe-Phen-C	37.60	21.91	24.77	15.72
Fe-N-C-800	44.00	21.02	22.13	12.85

Table S3. Summary of the Fe-N-C catalysts for ORR in alkaline medium.

Materials	$E_{1/2}$ (V) in 0.1 M KOH	References
Fe-N-C-800	0.883 (vs.RHE)	This work
Fe-N-C	0.82 (vs.RHE)	1
FeHis-700	0.86 (vs.RHE)	2
Fe@C-NG/NCNTs	0.84 (vs.RHE)	3
Fe-Fe ₃ C@C/CNT_Urea	0.87 (vs.RHE)	4
Fe ₃ C/NG-800	0.86 (vs.RHE)	5
FeNC-850	-0.152 (vs.Ag/AgCl)	6
Fe ₃ C/Fe@G-800	0.80 (vs.RHE)	7
Fe-N-C/rGO	0.81 (vs.RHE)	8
Fe3-NG	0.837 (vs.RHE)	9
Fe/N/APC-900	0.88 (vs.RHE)	10
Fe@N-doped graphene	0.851 (vs.RHE)	11
SA-Fe-HPC	0.89 (vs.RHE)	12
FeNx-PNC	0.86 (vs.RHE)	13
Fe-N/C-700	0.84 (vs.RHE)	14
Fe-Phen-N-800	0.86 (vs.RHE)	15
FeN ₂ /NOMC-3	0.863 (vs.RHE)	16
Fe-N/MPC2	0.88 (vs.RHE)	17

Table S4. Summary of the Fe-N-C catalysts for ORR in acidic medium.

Materials	$E_{1/2}$ (V)	References
Fe-N-C-800	0.723 (vs.RHE) in 0.1 M HClO ₄	This work
Fe-N-C	0.54 (vs.RHE) in 0.1 M HClO ₄	1
Fe ₃ C/NG-800	0.77 (vs.RHE) in 0.1 M HClO ₄	5
Fe-N/C-700	0.672 (vs.RHE) in 0.1 M HClO ₄	14
Fe-Phen-N-800	0.71 (vs.RHE) in 0.1 M HClO ₄	15
Fe-N/MPC2	0.70 (vs.RHE) in 0.5 M H ₂ SO ₄	17
Fe/C-700	0.70 (vs.RHE) in 0.1 M HClO ₄	18
Core/shell NPME	0.75 (vs.RHE) in 0.1 M HClO ₄	19
Fe ₃ C/C-700	0.73 (vs.RHE) in 0.1 M HClO ₄	20

Table S5. A survey of the performance of primary Zn-air batteries with Fe-based catalysts.

Materials	Peak power density (mW cm ⁻²)	Open-circuit potential (V)	References
Fe-N-C-800	135.3	1.476	This work
Fe@C-NG/NCNTs	101.3	1.37	3
FeNC-1000	55	1.42	21
S,N-Fe/N/C-CNT	102.7	1.35	22
3C-900	97	1.43	23
HP-Fe-N/CNFs	135	1.42	24
N-GCNT/FeCo	89.3	1.48	25
FeCo@MNC	115	1.41	26
Fe/Co-N/S-C	102.63	1.395	27

References

- 1 X. Yan, K. Liu, T. Wang, Y. You, J. Liu, P. Wang, X. Pan, G. Wang, J. Luo and J. Zhu, *J. Mater. Chem. A*, 2017, **5**, 3336-3345.
- 2 Y. Ding, Y. Niu, J. Yang, L. Ma, J. Liu, Y. Xiong and H. Xu, *Small*, 2016, **12**, 5414-5421.
- 3 Q. Wang, Y. Lei, Z. Chen, N. Wu, Y. Wang, B. Wang and Y. Wang, *J. Mater. Chem. A*, 2018, **6**, 516-526.
- 4 J. H. Kim, Y. J. Sa, H. Y. Jeong and S. H. Joo, *ACS Appl. Mater. Inter.*, 2017, **9**, 9567-9575.
- 5 M. Xiao, J. Zhu, L. Feng, C. Liu and W. Xing, *Adv. Mater.*, 2015, **27**, 2521-2527.
- 6 J. Yang, J. Hu, M. Weng, R. Tan, L. Tian, J. Yang, J. Amine, J. Zheng, H. Chen and F. Pan, *ACS Appl. Mater. Inter.*, 2017, **9**, 4587-4596.
- 7 A. Song, L. Cao, W. Yang, Y. Li, X. Qin and G. Shao, *ACS Sustain. Chem. Eng.*, 2018, **6**, 4890-4898.

- 8 C. Zhang, J. Liu, Y. Ye, Z. Aslam, R. Brydson and C. Liang, *ACS Appl. Mater. Inter.*, 2018, **10**, 2423-2429.
- 9 X. Cui, S. Yang, X. Yan, J. Leng, S. Shuang, P. M. Ajayan and Z. Zhang, *Adv. Funct. Mater.*, 2016, **26**, 5708-5717.
- 10 J. Xu, C. Wu, Q. Yu, Y. Zhao, X. Li and L. Guan, *ACS Sustain. Chem. Eng.*, 2017, **6**, 551-560.
- 11 D. Liu, C. Wu, S. Chen, S. Ding, Y. Xie, C. Wang, T. Wang, Y. A. Haleem, Z. Ur Rehman, Y. Sang, Q. Liu, X. Zheng, Y. Wang, B. Ge, H. Xu and L. Song, *Nano Res.*, 2018, **11**, 2217-2228.
- 12 Z. Zhang, J. Sun, F. Wang and L. Dai, *Angew. Chem., Int. Ed.*, 2018, **57**, 9038-9043.
- 13 L. Ma, S. Chen, Z. Pei, Y. Huang, G. Liang, F. Mo, Q. Yang, J. Su, Y. Gao, J. A. Zapien and C. Zhi, *ACS Nano*, 2018, **12**, 1949-1958.
- 14 Z. K. Yang, L. Lin and A. Xu, *Small*, 2016, **12**, 5710-5719.
- 15 Z. K. Yang, Z. Zhao, K. Liang, X. Zhou, C. Shen, Y. Liu, X. Wang and A. Xu, *J. Mater. Chem. A*, 2016, **4**, 19037-19044.
- 16 H. Shen, E. Gracia-Espino, J. Ma, H. Tang, X. Mamat, T. Wagberg, G. Hu and S. Guo, *Nano Energy*, 2017, **35**, 9-16.
- 17 L. Osmieri, R. Escudero-Cid, M. Armandi, A. H. A. Monteverde Videla, J. L. García Fierro, P. Ocón and S. Specchia, *Appl. Catal. B Environ.*, 2017, **205**, 637-653.
- 18 Y. Hu, J. O. Jensen, W. Zhang, S. Martin, R. Chenitz, C. Pan, W. Xing, N. J. Bjerrum and Q. Li, *J. Mater. Chem. A*, 2015, **3**, 1752-1760.
- 19 J. Li, Y. Song, G. Zhang, H. Liu, Y. Wang, S. Sun and X. Guo, *Adv. Funct. Mater.*, 2017, **27**, 1604356.
- 20 Y. Hu, J. O. Jensen, W. Zhang, L. N. Cleemann, W. Xing, N. J. Bjerrum and Q. Li, *Angew. Chem., Int. Ed.*, 2014, **53**, 3675-3679.
- 21 G. Ren, L. Gao, C. Teng, Y. Li, H. Yang, J. Shui, X. Lu, Y. Zhu and L. Dai, *ACS Appl. Mater. Inter.*, 2018, **10**, 10778-10785.
- 22 P. Chen, T. Zhou, L. Xing, K. Xu, Y. Tong, H. Xie, L. Zhang, W. Yan, W. Chu, C. Wu and Y. Xie, *Angew. Chem., Int. Ed.*, 2017, **56**, 610-614.
- 23 C. Li, H. Liu and Z. Yu, *Appl. Catal. B Environ.*, 2019, **241**, 95-103.
- 24 C. Li, M. Wu and R. Liu, *Appl. Catal. B Environ.*, 2019, **244**, 150-158.
- 25 T. Li, Y. Lu, S. Zhao, Z. Gao and Y. Song, *J. Mater. Chem. A*, 2018, **6**, 3730-3737.
- 26 C. Su, H. Cheng, W. Li, Z. Liu, N. Li, Z. Hou, F. Bai, H. Zhang and T. Ma, *Adv. Energy Mater.*, 2017, **7**, 1602420.
- 27 Y. Zhao, Q. Lai, Y. Wang, J. Zhu and Y. Liang, *ACS Appl. Mater. Inter.*, 2017, **9**, 16178-16186.